12 Solutions to Exercises

1.1 Beam Emittance in terms of Action Angle Variables

From (1.12) at a fixed location s we can write $x = \sqrt{2I_x\beta_x}\cos\phi_x$, where ϕ_x includes the initial phase ϕ_0. We then have

$$\begin{aligned}\epsilon_x &= \frac{\langle x^2(s)\rangle}{\beta_x(s)} \\ &= \int \mathrm{d}\phi_x\,\mathrm{d}I_x 2I_x\cos^2\phi_x\rho(I_x,\phi_x) \\ &= \int \mathrm{d}\phi_x\,\mathrm{d}I_x 2I_x\cos^2\phi_x\rho(I_x)\frac{1}{2\pi} \\ &= \int \mathrm{d}I_x I_x\rho(I_x) = \langle I_x\rangle\,. \end{aligned} \tag{12.1}$$

1.2 Projected Beam Emittances

a) The beam matrix after the skew quadrupole is

$$\Sigma^{xy}_{\mathrm{beam}} = \begin{pmatrix} \beta_x\epsilon_{x0} & 0 & 0 & K_s\beta_x\epsilon_{x0} \\ 0 & \epsilon_{x0}/\beta_x + K_s^2\epsilon_{y0}\beta_y & K_s\beta_y\epsilon_{y0} & 0 \\ 0 & K_s\beta_y\epsilon_{y0} & \beta_y\epsilon_{y0} & 0 \\ K_s\beta_x\epsilon_{x0} & 0 & 0 & \epsilon_{y0}/\beta_y + K_s^2\epsilon_{x0}\beta_x \end{pmatrix}. \tag{12.2}$$

b) The projected emittances are

$$\epsilon_x = \epsilon_{x0}\sqrt{1+\beta_x\beta_y K_s^2\frac{\epsilon_{y0}}{\epsilon_{x0}}}\,, \tag{12.3}$$

$$\epsilon_y = \epsilon_{y0}\sqrt{1+\beta_x\beta_y K_s^2\frac{\epsilon_{x0}}{\epsilon_{y0}}}\,. \tag{12.4}$$

2.1 Schottky Signals

a) The spectrum corresponds to lines of equal amplitude spaced either by $2\pi/\omega_{\mathrm{rev}}$, in time domain, or by $\omega_{\mathrm{rev}}/(2\pi)$ in frequency domain.

b) Since $\langle\cos n\omega_{\mathrm{rev},k}t\rangle_t = 0$, the average current is given by $e\sum_{k=1}^{N} f_{\mathrm{rev},k} \approx eNf_{\mathrm{rev}}$, where f_{rev} is the average revolution frequency of the particles.

c) The time average of the mixed terms $\cos(n\omega_{\mathrm{rev},k}t+\phi_k)\cos(n\omega_{\mathrm{rev},l}t+\phi_l)$ with $k \neq l$ is zero. The only terms with nonzero average in $(\sum_k i_k)^2$ are

M. G. Minty et al., *Measurement and Control of Charged Particle Beams,*
https://doi.org/10.1007/978-3-662-08581-3_12

$\sum_{k=1}^{N} \langle \cos^2(n\omega_{\mathrm{rev},k} t + \phi_k) \rangle_t = N/2$. After taking the square root, we obtain the desired result.

2.2 Betatron Tunes

a) The synchrotron tune is about $Q_s = 0.125$. (This is much higher than typical for lower-energy storage rings.)

b) The horizontal betatron tune is about $Q_x = 0.266$. The fact that the tune moves to the right by increasing the horizontally focusing quadrupoles shows that the tune lies between 0 and 0.5.

c) A particles would return to the same place in longitudinal phase space after $1/Q_s \approx 8$ turns, and to the same place in horizontal phase space after about $4/Q_x \approx 15$ turns.

2.3 Application of Multipole Field Expansion

a) For $b_2 \neq 0$ and $a_n = 0$ we have $B_y = B_0 b_2 (x^2 - y^2)$ and $B_x = 2B_0 b_2 xy$. Assuming that the particle is relativistic and moves longitudinally at the speed of light, the Lorentz force is $F_x = -cqB_y$ and $F_y = cqB_x$, where q is the particle charge.

b) Inserting a horizontal and vertical orbit offset, we find the aditional field components $\Delta B_y = 2B_0 b_2 (x_{\mathrm{co}} x_\beta - y_{\mathrm{co}} y_\beta)$ and $\Delta B_x = 2B_0 b_2 (y_{\mathrm{co}} x_\beta + x_{\mathrm{co}} y_\beta)$. It is easily verified that the field components proportional to x_{co} have the same dependence on x_β and y_β as one obtains for a normal quadrupole b_1, while those proportional to $y_{\mathrm{co}} \neq 0$ equal those for a skew quadrupole a_1.

c) If the dispersive contributions to the horizontal and vertical orbit ($x_\delta = D_x \delta$ and $y_\delta = D_y \delta$) are also included, the sextupole b_2 produces additional coupling terms $F_y \propto (x_\beta D_y \delta + y_\beta D_x \delta)$, and $F_x \propto (x_\beta D_x \delta + y_\beta D_y \delta)$.

2.4 Beta-Beat

a) The trace of the matrix product $R = R_Q R R_q$ is $\mathrm{Tr} R = 2\cos\phi_0 - \frac{\beta}{f}\sin\phi_0$. This must also be equal to $2\cos\phi$, from which follows that

$$\cos\phi = \cos\phi_0 - \frac{\beta_0}{2f}\sin\phi_0 \,. \tag{12.5}$$

b) In Fig. 2.9, the maximum phase advance error $\pm\Delta\phi$ is about $\pm 5^\circ$ or ± 0.087 rad. The beta beat oscillates at twice the betatron frequency. The design phase advance per arc cell is $\pi/2$. Thus, the length of an arc cell corresponds to the distance between a location at which the phase equals the (local) average value and the next maximum in $\Delta\phi$. If the optics error is not introduced in this region of the ring, the perturbed R_{12} optical transport matrix element $\sqrt{\hat{\beta}\beta_0}\sin(\pi/2 + \Delta\phi)$ between these two locations is equal to the design matrix element $R_{12,0} = \beta_0 \sin\pi/2 = \beta_0$. From this equality, we can infer that

$$\frac{\hat{\beta}}{\beta_0} = \frac{\sin^2 \pi/2}{\sin^2(\pi/2 + \Delta\phi)} \,, \tag{12.6}$$

or $(\hat{\beta} - \beta_0)/\beta_0 \approx 0.8\%$.

2.5 Quadrupole with a Shorted Coil

a) The upper inboard coil is suspected of a short.

b) The faulted coil gives rise to an additional dipole-like deflection of angle $\Delta\theta \approx \Delta B l_q/(B\rho) = (\Delta B/B)aK$, where ΔB is proportional to the field change ΔI through this coil. The deflection is measured a distance l downstream at a BPM with resolution Δx. The relative change in the coil current I can then be determined with a resolution of $\Delta I/I \propto \Delta B/B = \Delta x/(Kla) \approx 10^{-3}$.

2.6 Quadrupole Gradient Errors

a) The π bump is made from two correctors separated by a total betatron phase advance of π. The first corrector applies a deflection of angle θ_1. This results in an offset $\Delta x = \sqrt{\beta_1\beta_q}\sin\phi_{1q}$ at the quadrupole, where β_1 is the beta function at the corrector, β_q that at the quadrupole and ϕ_{1q} the phase advance from the corrector to the quadrupole. The second corrector at a location with beta function β_2 and a phase advance ϕ_{q2} behind the quadrupole gives rise to a deflection angle θ_2:

$$\theta_2 = -\theta_1\sqrt{\frac{\beta_1}{\beta_2}}(\cos\phi_{12} - \alpha_2\sin\phi_{12}) = \theta_1\sqrt{\frac{\beta_1}{\beta_2}}\,. \tag{12.7}$$

Since the two correctors are located exactly π apart there is no residual oscillation.

b) The gradient error ΔK gives rise to an additional deflection $\Delta\theta = \Delta K\,\Delta x = \Delta K\sqrt{\beta_1\beta_q}\sin\phi_{1q}\theta_1$, at the quadrupole, which translates into an offset

$$\Delta x_2 = \Delta\theta\sqrt{\beta_2\beta_q}\sin\phi_{q2} = \Delta K\beta_q\sqrt{\beta_2\beta_1}\sin\phi_{q2}\sin\phi_{1q}\theta_1 \tag{12.8}$$

at the location of the second corrector. Denoting the normalized residual amplitude by $A = \Delta x_2/(\sqrt{\beta_2}\sin\phi_{q2})$ and find

$$A = \Delta K(\beta_q\sqrt{\beta_1}\sin\phi_{1q})\theta_1\,, \tag{12.9}$$

which relates the measured leakage A to the gradient error ΔK.

2.7 Multiknobs

We compute or measure the 2×2 sensitivity matrix S relating the strengths of the two quadrupole families (ΔK_1 and ΔK_2) and the changes in the two tunes:

$$\begin{pmatrix}\Delta Q_x\\ \Delta Q_y\end{pmatrix} = \begin{pmatrix}S_{11} & S_{12}\\ S_{21} & S_{22}\end{pmatrix}\begin{pmatrix}\Delta K_1\\ \Delta K_2\end{pmatrix}\,. \tag{12.10}$$

Next, we invert the matrix S,

$$\begin{pmatrix}\Delta K_1\\ \Delta K_2\end{pmatrix} = \frac{1}{\det S}\begin{pmatrix}S_{22} & -S_{12}\\ -S_{21} & S_{11}\end{pmatrix}\begin{pmatrix}\Delta Q_x\\ \Delta Q_y\end{pmatrix}\,. \tag{12.11}$$

From this equation, we obtain the linear combinations of ΔK_1 and ΔK_2 for which $\Delta Q_x \neq 0$ and $\Delta Q_y = 0$, or vice versa.

3.1 Design of an Orbit Feedback Loop

a) The two correctors are placed at two different locations upstream of the BPMs. We design a feedback loop which adjusts the strength of the two correctors so that the beam position is zero. Denoting the beam positions measured at the two BPMs without feedback correction by x_1 and x_2, the equations for the feedback loop are

$$x_1 + C_{k1,1}\theta_1 + C_{k2,1}\theta_2 = 0\,, \tag{12.12}$$
$$x_2 + C_{k1,2}\theta_1 + C_{k2,2}\theta_2 = 0\,, \tag{12.13}$$

where θ_1 and θ_2 are the deflection angles applied by the two correctors, and the coefficients

$$C_{ki,j} = \sqrt{\beta_{ki}\beta_j}\sin\phi_{ki,j} \quad \text{for} \quad i,j = 1,2\,, \tag{12.14}$$

are the (1,2) transfer matrix elements between the ith corrector and the jth BPM, and $\phi_{ki,j}$ the associated betatron phase advance. Combining (12.12) and (12.13) and solving for either θ_1 or θ_2, we obtain

$$\theta_2 = \frac{C_{k1,2}x_1 - C_{k1,1}x_2}{C_{k2,1,}C_{k1,2} - C_{k2,2}C_{k1,1}} \tag{12.15}$$
$$= \frac{1}{\sqrt{\beta_{k2}}}\,\frac{x_1\sin\phi_{k1,2}/\sqrt{\beta_1} - x_2\sin\phi_{k1,1}/\sqrt{\beta_2}}{\sin\phi_{k2,1}\sin\phi_{k1,2} - \sin\phi_{k2,2}\sin\phi_{k1,1}}\,, \tag{12.16}$$
$$\theta_1 = \frac{C_{k2,2}x_1 - C_{k2,1}x_2}{C_{k1,1,}C_{k2,2} - C_{k1,2}C_{k2,1}} \tag{12.17}$$
$$= \frac{1}{\sqrt{\beta_{k1}}}\,\frac{x_1\sin\phi_{k2,2}/\sqrt{\beta_1} - x_2\sin\phi_{k2,1}/\sqrt{\beta_2}}{\sin\phi_{k1,1}\sin\phi_{k2,2} - \sin\phi_{k1,2}\sin\phi_{k2,1}}\,. \tag{12.18}$$

The phase advances between the correctors and the BPMs should not be all equal to 0 or π. In particular, $\sin\phi_{ki,1}$ and $\sin\phi_{ki,2}$ should not be both equal to 0, for $i = 1$ or 2, and $\sin\phi_{k1,j}$ and $\sin\phi_{k2,j}$ shoud not be both equal to zero, as otherwise neither corrector would affect the orbit reading at BPM j. Moreover, the ratios of coefficients $C_{k1,2}/C_{k1,1}$ and $C_{k2,2}/C_{k2,1}$ should not be equal, to avoid a degeneracy and an identical effect of the two correctors. Note that in the extreme case of $C_{k1,2} = 0$ and $C_{k2,1} = 0$, corrector 1 only interacts with BPM 1 and corrector 2 only with BPM 2. The beta functions should be large at the correctors, which minimizes the corrector strength required, and they should also large at the BPMs, which maximizes the sensitivity to orbit changes.

b) In the case of a storage ring, (12.15) and (12.17) still apply, but the coefficients $C_{ki,j}$ now follow from the formula for the closed-orbit distortion (2.34):

$$C_{ki,j} = \frac{\sqrt{\beta_{ki}\beta_j}\cos(|\phi_{ki,j}| - \pi Q_x)}{2\sin\pi Q_x} \quad \text{for} \quad i,j = 1,2\,, \tag{12.19}$$

where Q is the betatron tune, and $\phi_{ki,j}$ as before denotes the betatron phase advance from corrector i to BPM j. The dependence on the beta functions is the same as for a transport line, but the optimum phase advance between the correctors and BPMs now depends on the betatron tune. Again, the ratios of the coefficients $C_{k1,2}/C_{k1,1}$ and $C_{k2,2}/C_{k2,1}$ should be different, to avoid degeneracy.

3.2 Linac Dispersion and Orbit Correction

a) Equation (3.48) describes a harmonic oscillator. The solution is [1]

$$x_1(s) = \frac{\theta}{k_\beta\sqrt{1+\delta_1}} \sin\frac{k_\beta s}{\sqrt{1+\delta_1}} \approx \frac{\theta}{k_\beta\sqrt{1+\delta_1}} \left[\sin k_\beta s - \frac{1}{2} k_\beta s \delta_1 \cos k_\beta s\right] \tag{12.20}$$

or

$$x_1(s) \approx \frac{\theta}{k_\beta} \sin k_\beta s - \frac{1}{2}\left[\theta s \cos k_\beta s + \frac{\theta}{k_\beta} \sin k_\beta s\right] \delta_1 + \mathcal{O}(\delta_1^2)\,. \tag{12.21}$$

From the term linear in δ_1 we infer the dispersion at the bunch head,

$$D_1(s) = -\frac{1}{2}\left[\theta s \cos k_\beta s + \frac{\theta}{k_\beta} \sin k_\beta s\right]\,. \tag{12.22}$$

The solution is illustrated in Fig. 12.1. The linear increase with s reflects that the dispersion is resonantly driven [1].

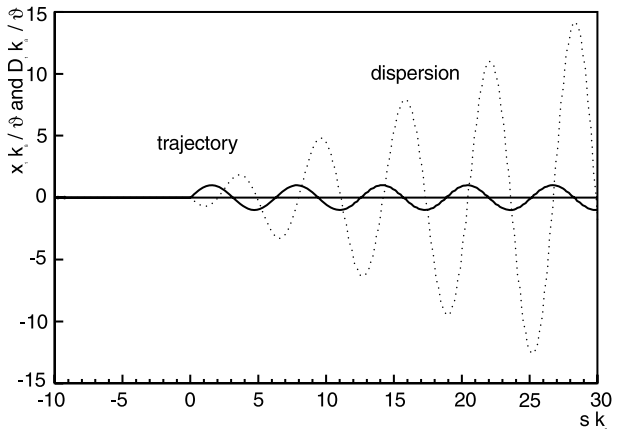

Fig. 12.1. Trajectory oscillation, $x_1 k_\beta/\theta$ for $\delta_1 = 0$, and resonantly growing dispersion at the bunch head, $D_1 k_\beta/\theta$, induced by a deflection at $s = 0$, according to (12.21) and (12.22)

b) The dispersion generated by a single kick at $s = 0$, $D_1(s)$, was computed in (12.22). The dispersion generated by the second kick is obtained by

simply shifting the argument by s_2, i.e., it is given by $D_1(s - \pi/k_\beta)$. The dispersion arising from the π bump is then the sum of the terms generated by the two kicks [1]:

$$D_\pi = D_1(s) + D_1(s - \pi/k_\beta) = -\frac{\theta\pi}{2k_\beta} \cos k_\beta s \,. \tag{12.23}$$

The solution is illustrated in Fig. 12.2. While the orbit after the π bump is zero, the dispersion propagates at a constant amplitude. A perfectly centered orbit in the downstream linac section does not imply that the dispersion is zero as well.

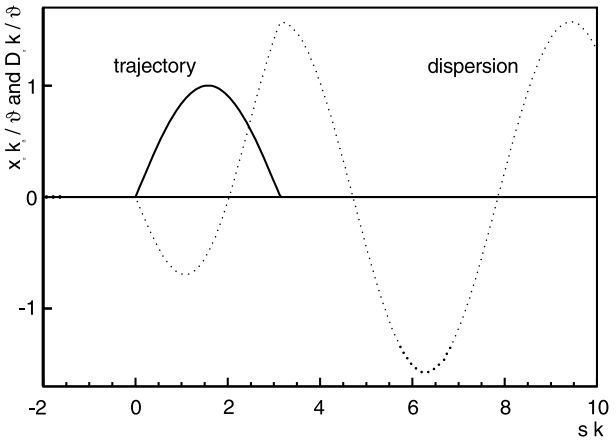

Fig. 12.2. Trajectory perturbation, $x_\pi k_\beta/\theta$, and subsequent constant dispersion, $D_\pi k_\beta/\theta$, induced by a π bump, according to (12.23)

4.1 Beta Mismatch

From (1.15), the action variable of a particle with respect to the matched design optics (subindex 'D') is

$$I = \frac{x^2 + (\beta_D x' + \alpha_D x)^2}{2\beta_D} \,. \tag{12.24}$$

After filamentation and phase randomization the average action is equal to the rms emittance (see (1.14)), i.e., $\epsilon = \langle I \rangle_{\rm f} = \langle x^2 \rangle_{\rm f}/\beta_D$ where the subindex f refers to averaging after filamentation. In a linear system I is conserved, and, hence, its initial average value $\langle I \rangle$ does not change, or $\langle I \rangle = \langle I \rangle_{\rm f}$. Averaging I over the initial distribution and using the relations $\langle x^2 \rangle = \beta\epsilon_0$, $\langle x'^2 \rangle = \gamma\epsilon_0$, and $\langle xx' \rangle = -\alpha\epsilon_0$, we then obtain the final emittance

$$\epsilon = \langle I \rangle = \frac{\gamma_D\beta - 2\alpha_D\alpha + \beta_D\gamma}{2} \, \epsilon_0 = B_{\rm mag}\epsilon_0 \,. \tag{12.25}$$

4.2 Propagation of Twiss Parameters

Let the initial phase-space ellipse be

$$\gamma_0 x(0)^2 + 2\alpha_0 x(0)x'(0) + \beta_0 x'(0)^2 = \epsilon\,. \tag{12.26}$$

In this case ϵ is not the rms beam emittance, but it describes the phase-space area enclosed by the ellipse. Except for a factor 2 this area is equal to the action variable of a particle located on the ellipse, and, in particular, it is a conserved quantity under linear beam transport.

We can evaluate the phase space ellipse at a later location s, namely

$$\gamma_s x(s)^2 + 2\alpha_s x(s)x'(s) + \beta_s x'(s)^2 = \epsilon\,. \tag{12.27}$$

Now the trick is to express the initial parameters $x(0)^2$, $x(0)x'(0)$, and $x'(0)^2$ in terms of the final quantities $x(s)^2$, $x(s)x'(s)$, and $x'(s)^2$ using the inverse transport matrix between the two locations:

$$\begin{aligned} x(0)^2 &= S'^2 x(s)^2 - 2S'Sx(s)x'(s) + S^2 x'(s)^2 \\ x(0)x'(0) &= -S'C'x(s)^2 - SCx'(s)^2 - (SC + S'C')x(s)x'(s) \\ x'(0)^2 &= C'^2 x(s)^2 - 2C'Cx'(s)x'(s) + S^2 x'(s)^2\,. \end{aligned}$$

Inserting the last expressions into (12.26), expanding the products, and comparing coefficients of x_0^2, $x_0x'(0)$, and $x'(0)^2$ with those in (12.27), we arrive at the desired result:

$$\begin{pmatrix} \gamma_s \\ \alpha_s \\ \beta_s \end{pmatrix} = \begin{pmatrix} S^2 & -2S'C' & C'^2 \\ -SS' & SC' + S'C & -CC' \\ S^2 & -2SC & C^2 \end{pmatrix} \begin{pmatrix} \gamma_0 \\ \alpha_0 \\ \beta_0 \end{pmatrix}\,. \tag{12.28}$$

4.3 Static and Dynamic change of Partition Numbers

a) We apply (4.82)

$$\Delta\mathcal{D} \approx -\left(\sum_q k_q^2 D_{x,q} L_q\right) \frac{2\rho^2}{C}\, \Delta x^{\mathrm{mag}}\,, \tag{12.29}$$

which gives $\Delta\mathcal{D} = -0.16$ (16% change) for $\Delta x^{\mathrm{mag}} = 1.5$ mm.

b) From (4.83) we estimate the equivalent change in the rf frequency as

$$\Delta f_{\mathrm{rf}} \approx f_{\mathrm{rf}} \frac{2\pi \Delta x^{\mathrm{mag}}}{C}\,, \tag{12.30}$$

and obtain $\Delta f_{\mathrm{rf}} \approx 192$ kHz.

4.4 Effect of Wiggler on Equilibrium Emittance

Rewriting (4.103) und using $\theta_w = \lambda_p/(\rho_w 2\pi)$, we have

$$\begin{aligned}\gamma\epsilon_{x,w} &\approx \frac{16}{30\pi}\frac{C_q\beta_x}{\rho_w}\gamma^3\theta_w^2 \\ &= \frac{16}{30\pi}\frac{C_q\beta_x}{\rho_w^3}\gamma^3\frac{\lambda_p^2}{(2\pi)^2} \\ &\approx 3.3\times 10^{-16}\ \mathrm{m}^4\ \frac{\gamma^3 B_w^3}{(B\rho)^3} \\ &\approx 4.2\ \mu\mathrm{m}\,,\end{aligned} \tag{12.31}$$

where $(B\rho)$ is the magnetic rigidity. The normalized emittance is independent of the beam energy. Applying (4.105),

$$\tau_{x,w} \approx \frac{2\rho_w^2}{C_d J_x E^3}\,, \tag{12.32}$$

with $C_d \approx 2.1\times 10^3\ \mathrm{m^2GeV^{-3}s^{-1}}$ and $J_x = 1$, yields a damping time of 670 μs at 1 GeV and about 130 μs at 5 GeV.

The normalized emittance is about the same as in a typical damping ring design for a future linear collider, but the damping time is 5–20 times shorter.

4.5 BNS Damping at the SLC

From (4.112), we have $\xi \approx -1.27$. Combining the generalization of (4.110) to accelerated beams and (4.111) yields

$$\delta_{\mathrm{BNS}} = \frac{N_b r_e \beta^2 W_1(z)}{4L\xi}\ \frac{\ln(\gamma_f/\gamma_i)}{\gamma_f}\,, \tag{12.33}$$

where γ_f and γ_i refer to the final and initial beam energy, respectively. Inserting numbers, we find $\delta_{\mathrm{BNS}} \approx -0.1$, or a 10% energy spread across the bunch.

5.1 Solenoidal Focusing

The phase-space coordinates after the distance z_f are

$$r'(z_f) = \Lambda z_f \tag{12.34}$$

$$r(z_f) \ = \frac{1}{2}\Lambda z_f^2 + r_0\,, \tag{12.35}$$

where, for simplicitiy, we have dropped the arguments ρ and ξ of r, r' and Λ. After passing through the lens of focal length f and traversing a further distance z_d, we have

$$r'(z_f + z_d) = \Lambda z_f - \frac{1}{f}\left(\frac{1}{2}\Lambda z_f^2 + r_0\right) + \Lambda z_d \tag{12.36}$$

$$\begin{aligned} r(z_f) \qquad &= \frac{1}{2}\Lambda z_f^2 + r_0 + z_d z_f \Lambda \\ &\quad -\frac{1}{f} z_d \left(\frac{1}{2}\Lambda z_f^2 + r_0\right) + \frac{1}{2}\Lambda z_d^2\,. \end{aligned} \tag{12.37}$$

Inserting $f = z_d^2/(2(z_f + z_d))$ and rearranging terms gives

$$r'(z_f + z_d) = \frac{2(z_f + z_d)}{z_d^2}\left[-\frac{1}{2}\Lambda z_f\left(z_f - \frac{z_d^2}{z_f}\right) - r_0\right] \tag{12.38}$$

$$r(z_f + z_d) = \left(1 + 2\frac{z_f}{z_d}\right)\left[-\frac{1}{2}\Lambda z_f\left(z_f - \frac{z_d^2}{z_f}\right) - r_0\right]. \tag{12.39}$$

Dividing (12.38) by (12.39) yields the desired result.

5.2 Flat-Beam Transformer

a) For $\mu = 2\pi$, $\Delta = -\pi/2$, and $\alpha = 0$, the matrices A and B are

$$A = I\cos 2\pi + J\sin 2\pi = I \tag{12.40}$$

$$B = I\cos(3\pi/2) + J\sin(3\pi/2) = -J \tag{12.41}$$

The matrix M in (5.18) becomes

$$M = \frac{1}{2}\begin{pmatrix} 1 & -\beta & 1 & \beta \\ 1/\beta & 1 & -1/\beta & 1 \\ 1 & \beta & 1 & -\beta \\ -1/\beta & 1 & 1/\beta & 1 \end{pmatrix} = M = \frac{1}{2}\begin{pmatrix} 1 & -1/k & 1 & 1/k \\ k & 1 & -k & 1 \\ 1 & 1/k & 1 & -1/k \\ -k & 1 & k & 1 \end{pmatrix}, \tag{12.42}$$

where we have used $\beta = 1/k$.

b) Multiplying the matrix M and the vector (5.24), we obtain the final coordinates

$$\begin{pmatrix} x \\ x' \\ y \\ y' \end{pmatrix}_1 = \frac{1}{2}\begin{pmatrix} 1 & -1/k & 1 & 1/k \\ k & 1 & -k & 1 \\ 1 & 1/k & 1 & -1/k \\ -k & 1 & k & 1 \end{pmatrix}\begin{pmatrix} x_0 \\ -ky_0 + x_0' \\ y_0 \\ kx_0 + y_0' \end{pmatrix}. \tag{12.43}$$

The equations for y_1 and y_1' are

$$y_1 = \frac{1}{2k}(x_0' - y_0') \tag{12.44}$$

$$y_1' = \frac{1}{2}(x_0' + y_0'), \tag{12.45}$$

from which we obtain the second moments

$$\langle y_1^2\rangle = \frac{1}{4k^2}\left(\sigma'^2_{x0} + \sigma'^2_{y0}\right) \tag{12.46}$$

$$\langle y_1 y_1'\rangle = \frac{1}{4}\left(\sigma'^2_{x0} - \sigma'^2_{y0}\right) = 0 \tag{12.47}$$

$$\langle y_1'^2\rangle = \frac{1}{4}\left(\sigma'^2_{x0} + \sigma'^2_{y0}\right). \tag{12.48}$$

The final vertical rms emittance is

$$\epsilon_{y,1} = \sqrt{\langle y_1^2\rangle\langle {y'}_1^2\rangle - \langle y_1 {y'}_1\rangle^2} = \frac{{\sigma'}_{y0}^2}{2k}\,, \tag{12.49}$$

which demonstrates (5.25). The equations for x_1 and x_1' are

$$x_1 = x_0 + y_0 - \frac{x_0'}{2k} + \frac{y_0'}{2k} \tag{12.50}$$

$$x_1' = k(x_0 - y_0) + \frac{1}{2}(x_0' + y_0')\,. \tag{12.51}$$

In this case, the second moments are

$$\langle x_1^2\rangle \;\; = 2\sigma_{x0}^2 + \frac{{\sigma'}_{x0}^2}{2k^2} \tag{12.52}$$

$$\langle x_1 x_1'\rangle = 0 \tag{12.53}$$

$$\langle {x'}_1^2\rangle \;\; = 2k^2\sigma_{x0}^2 + \frac{1}{2}{\sigma'}_{x0}^2\,. \tag{12.54}$$

The final horizontal rms emittance is

$$\begin{aligned}\epsilon_{x,1} &= \sqrt{\langle x_1^2\rangle\langle {x'}_1^2\rangle - \langle x_1 {x'}_1\rangle^2} \\ &= \sqrt{4k^2\sigma_{x0}^2 + 2\sigma_{x0}^2{\sigma'}_{x0}^2 + \frac{1}{4}{\sigma'}_{x0}^4\frac{1}{k^2}} \\ &= \sqrt{4k^2{\sigma_{x0}}^4 + 4k\epsilon_{y,1}\sigma_x^2 + \epsilon_{y,1}^2} \\ &= 2k\sigma_{x0}^2 + \epsilon_{y,1}\,. \end{aligned} \tag{12.55}$$

The last equation can also be written as

$$\frac{\epsilon_{x,1}}{\epsilon_{y,1}} = 1 + \frac{4k^2\sigma_{x0}^2}{{\sigma'}_{x0}^2}\,, \tag{12.56}$$

which confirms (5.26).

6.1 Scattering off Thermal Photons

a) The beam lifetime due to scattering off thermal photons is

$$\tau \approx \frac{1}{\rho_\gamma c\sigma_T}\,, \tag{12.57}$$

where $\rho_\gamma \approx 5\times 10^{14}$ m^{-3} denotes the photon density at 300 K, c the speed of light, and $\sigma_T \approx 0.67$ barn the Thomson cross section. This yields a beam lifetime of 28 hr.

b) The photon density varies with the third power of the temperature. If the vacuum chamber is cooled to 4 K, the beam lifetime increases to about 1400 years.

c) The number of particles lost per train is

$$\Delta N = L\sigma_T \rho_\gamma N \,, \tag{12.58}$$

where L is the length of the linac, ρ_γ the photon density, and N the total number of particles. Inserting numbers, for a chamber temperature of 300 K we find $\Delta N \approx 335$ lost particles.

7.1 Review of Fourier Transformations and an Application

a) For simplicity we initially set $\Delta t = 0$. The Fourier spectrum of the current signal is

$$\begin{aligned} I(\omega) &= \frac{1}{2\pi}\int_{-\infty}^{\infty} i(t) e^{-\mathrm{i}\omega t}\,\mathrm{d}t \\ &= \frac{Q}{2\pi}\int_{-\infty}^{\infty} \sum_{n=-\infty}^{\infty} \left[\delta\left[t - nT - \tau_a \cos(\omega_s nT)\right] e^{-\mathrm{i}\omega t}\right. \\ &\quad \left. + \delta\left[t - nT - \frac{T}{2} - \tau_a \cos(\omega_s nT + \phi)\right] e^{-\mathrm{i}\omega t}\,\mathrm{d}t. \right. \end{aligned} \tag{12.59}$$

Application of the given property of Delta-functions yields

$$\begin{aligned} I(\omega) &= \frac{Q}{2\pi} \sum_{n=-\infty}^{\infty} e^{-\mathrm{i}\omega[nT + \tau_a \cos(\omega_s nT)]} \\ &\quad + \frac{Q}{2\pi} \sum_{n=-\infty}^{\infty} e^{-\mathrm{i}\omega[nT + \frac{T}{2} + \tau_a \cos(\omega_s nT + \phi)]} \,. \end{aligned} \tag{12.60}$$

Using the Bessel function sum rule,

$$\begin{aligned} I(\omega) &= \frac{Q}{2\pi} \sum_{n,k=-\infty}^{\infty} e^{-\mathrm{i}\omega nT} (-i)^k J_k(\tau_a \omega) e^{\mathrm{i}k\omega_s nT} \\ &\quad + \frac{Q}{2\pi} \sum_{n,k=-\infty}^{\infty} e^{-\mathrm{i}\omega(nT + \frac{T}{2})} (-i)^k J_k(\tau_a \omega) e^{\mathrm{i}k(\omega_s nT + \phi)} \,. \end{aligned} \tag{12.61}$$

With $\omega_r T = 2\pi$, this becomes

$$\begin{aligned} I(\omega) &= \frac{Q}{2\pi} \sum_{n,k=-\infty}^{\infty} e^{-\mathrm{i}2\pi n\left(\frac{\omega - k\omega_s}{\omega_r}\right)} (-i)^k J_k(\tau_a \omega) \\ &\quad \left[1 + e^{-\mathrm{i}\left(\frac{\pi\omega}{\omega_r} - k\phi\right)}\right] \,, \end{aligned} \tag{12.62}$$

and using the Poisson sum rule, it further simplifies to

$$I(\omega) = Q\omega_r \sum_{n,k=-\infty}^{\infty} (-i)^k J_k(\tau_a \omega) \left[1 + e^{-\mathrm{i}\left(\pi\frac{\omega}{\omega_r} - k\phi\right)}\right] \delta(\omega - n\omega_r - k\omega_s) \,. \tag{12.63}$$

This expression shows that the spectrum contains the usual rotation harmonics ($k = 0$), and synchrotron sidebands ($k \neq 0$) where the height of the sidebands is given by the Bessel function of appropriate order k.

b) Dipole-mode oscillations correspond to $k = \pm 1$. Consider the phase factor, given in square brackets in (12.63), and the spectrum of sidebands with $k = 1$,

$$\left[1 + e^{-\mathrm{i}(\pi \frac{\omega}{\omega_r} - \phi)}\right] , \tag{12.64}$$

which is to be evaluated at $\omega = n\omega_r \pm \omega_s$. Assuming that $T\omega_s \ll 1$, we can neglect the imaginary part of this expression, and for the in-phase oscillations ($\phi = 0$) the real part of the phase factor approximately becomes

$$1 + \cos n\pi \approx \begin{cases} 2 & \text{for even } n \\ 0 & \text{for odd } n \end{cases} , \tag{12.65}$$

while for the out-of-phase oscillations ($\phi = \pi$),

$$1 + \cos n\pi \approx \begin{cases} 0 \text{ for even } n \\ 2 \text{ for odd } n \end{cases} . \tag{12.66}$$

Therefore, one can determine experimentally which of the two normal modes dominates by determining whether the sidebands are located around the even or odd revolution harmonics. The same results apply for $k = -1$.

c) Considering now unequal bunch spacings ($\Delta t \neq 0$), the phase factors become

$$1 + \cos n\pi \cos n\omega_r \Delta t \quad \text{for} \quad \phi = 0 \tag{12.67}$$

$$1 - \cos n\pi \cos n\omega_r \Delta t \quad \text{for} \quad \phi = \pi . \tag{12.68}$$

The location of a π-mode sideband for unequally spaced bunches may coincide with the location of a 0-mode sideband for equally spaced bunches, namely if

$$1 - \cos n\pi \cos n\omega_r \Delta t = 1 + \cos n\pi . \tag{12.69}$$

This condition is satisfied for

$$\Delta t = \frac{T}{2n} . \tag{12.70}$$

The SLC had two damping rings one with equally spaced bunches and the other with unequally spaced bunches (the bunches in this case were separated by 40 buckets and 44 buckets with harmonic number 84). To achieve a common design of "π-mode" cavity for both rings a compromise was made in selecting the cavity resonance frequency such that each ring had partial (though not fully efficient) damping of the π-modes.

7.2 Adjusting the Incoming Beam Energy

If the energy of the injected beam is not correct, it will undergo synchrotron oscillations. Let us assume that the initial relative momentum deviation is δ. The maximum change in the beam energy with respect to the

incoming energy occurs after half a synchrotron period, when the relative momentum error is $-\delta$. The orbit difference at a location with dispersion D_x is $\Delta x = -2D_x\delta$. Minimizing the difference orbit measured at this time with respect to the first turn corrects the energy of the injected beam.

If the 'matched' energy around which the injected beam oscillates does not coincide with a centered closed orbit, one may first have to adjust the ring rf frequency and, for protons or ions, the bending field, such that the equilibrium orbit in the ring is centered and corresponds to the correct energy. Afterwards one can then apply the procedure described above in order to adjust the injected beam energy.

If a longitudinal 'phase' monitor is available, another solution, for any type of beam, is to minimize the phase error measured after a quarter synchrotron period.

7.3 Resonant Depolarization

We can express the relative energy error as

$$\frac{\Delta E}{E} = \beta^2 \frac{\Delta p}{p} = \beta^2 \frac{1}{\alpha_c} \frac{\Delta C}{C}\,, \tag{12.71}$$

where β is the beam velocity in units of the speed of light (and not the beta function), α_c the momentum compaction factor, and C the ring circumference.

7.4 Approximate Expression for the Momentum Compaction Factor

a) We insert the approximate formula for the average dispersion into the definition of the momentum compaction factor, (7.22), and get

$$\begin{aligned} \alpha_c &= \frac{1}{C} \oint \frac{D_x(s)}{\rho(s)}\, \mathrm{d}s \approx \frac{1}{C} \oint \frac{\langle \beta_x \rangle}{Q_x \rho(s)}\, \mathrm{d}s \\ &\approx \frac{1}{C} \frac{\langle \beta_x \rangle}{Q_x} \frac{C}{\rho} = \frac{\langle \beta_x \rangle}{\rho} \frac{1}{Q_x} \approx \frac{1}{Q_x^2}\,, \end{aligned} \tag{12.72}$$

where in the last step we have used $Q_x = \oint \mathrm{d}s/\beta/(2\pi) \approx \rho/\langle \beta_x \rangle$. As an example, assuming $Q_x = 50$, we estimate that $\alpha_c \approx 1/Q_x^2 \approx 4 \times 10^{-4}$.

b) A corresponding expression for the transition energy γ_t is easily obtained:

$$\gamma_t = \frac{1}{\sqrt{\alpha_c}} = Q_x\,. \tag{12.73}$$

7.5 Achieving Design Parameters in the Presence of Unknowns

A possible set up is the following. The rf frequency ω_{rf} is known, and first set so as to horizontally center the beam at the beam position monitors in the steady state after a few radiation damping times. The rf frequency determines the revolution time. Since the electron beam moves at the speed of light, also the ring circumference is now determined.

The energy of the injected beam is set to the design value, and the magnetic field of the ring is adjusted until one observes no horizontal orbit variation at dispersive locations, or no longitudinal phase motion, due to synchrotron oscillations after injection. This might also require an adjustment of the rf phase, in order to avoid synchrotron oscillations due to injection phase errors, in addition to those from magnetic field errors. (The two types of errors can also be distinguished from the phase of the oscillation.)

Note that one possibility of measuring the energy of the injected beam is to monitor the orbit in a dispersive region of the injection transfer line, and its dependence on known step changes in the beam energy, e.g., generated by phasing a klystron.

The problem could be simplified, if additional information on the beam energy in the ring is available, e.g., by resonant depolarization or by a reaction with a target for which the cross section is sensitive to the energy.

7.6 Chromatic Phase Advance[1]

a) Keeping only terms up to order δ, with $x = x_\beta + D_x\eta$ and $y = y_\beta + D_y\eta$ with $D_y = 0$, (7.45) gives

$$\begin{aligned} {x_\beta}'' + kx_\beta &= kx_\beta\delta - mD_x x_\beta\delta - \frac{m}{2}({x_\beta}^2 - {y_\beta}^2)\,, \\ {y_\beta}'' - ky_\beta &= -ky_\beta\delta + mD_x y_\beta\delta + mx_\beta y_\beta\,. \end{aligned} \tag{12.74}$$

Keeping only the energy-dependent terms,

$$\begin{aligned} {x_\beta}'' + kx_\beta &= (k - mD_x)x_\beta\delta \\ {y_\beta}'' - ky_\beta &= -(k - mD_x)y_\beta\delta\,. \end{aligned} \tag{12.75}$$

b) In the present case, the horizontal focusing error for an off-energy particle is

$$\Delta k_x(s) = -(k - mD_x)\delta\,. \tag{12.76}$$

In the vertical plane, the focusing error is of opposite sign, $\Delta k_y(s) = -\Delta k_x(s)$. Inserting this into

$$\Delta Q = \frac{1}{4\pi}\int_s^{s+C} \beta(s)\Delta k(s)\,\mathrm{d}s\,, \tag{12.77}$$

and noting that $\Delta\phi = \Delta Q 2\pi$, we immediately have

$$\begin{aligned} \Delta\phi_x &= -\frac{\delta}{2}\int_s^{s+C} \beta_x(k - mD_x)\,\mathrm{d}s\,, \\ \Delta\phi_y &= \frac{\delta}{2}\int_s^{s+C} \beta_y(k - mD_x)\,\mathrm{d}s\,. \end{aligned} \tag{12.78}$$

[1] adapted from [31]

c) Using the definition of the chromaticity

$$Q'_{x,y} = \frac{\Delta Q}{\delta} = \frac{\Delta \phi_{x,y}}{2\pi\delta} , \tag{12.79}$$

and the expressions for $\Delta\phi_{x,y}$ derived in b), we obtain

$$\begin{aligned} Q'_x &= -\frac{1}{4\pi} \int \beta_x (k - mD_x)\, \mathrm{d}s \ , \\ Q'_y &= \frac{1}{4\pi} \int \beta_y (k - mD_x)\, \mathrm{d}s \ . \end{aligned} \tag{12.80}$$

8.1 Phase Tolerances in a Bunch Compressor

From (8.8) we have

$$\frac{\partial \phi_3}{\partial \phi_1} = 1 + R_{56} \frac{\omega_{\mathrm{rf}}}{c} \frac{eV}{E} \ . \tag{12.81}$$

The error in the final phase $\partial\phi_3$ as a function of error in the injection phase $\partial\phi_1$ therefore depends linearly on the compressor voltage. Minimum sensitivity is achieved for $\frac{\partial \phi_3}{\partial \phi_1} = 0$ or $V = 33.4$ MV.

8.2 Bunch Precompression

a) We assume that the bunch length is small compared to the wavelength of the accelerating rf. The bunch centroid is initially ($t < t_0$) at the center of phase space ($\delta = 0, \phi = 0$) and the phase space trajectories are elliptical centered about the bunch centroid with amplitude given by the voltage V_0. During the time $t_0 < t < t_1 = \frac{\tau_{s,l}}{8}$ the cavity voltage is lowered to 0.75 V_0. This introduces a shift in synchronous phase and the bunch centroid executes 1/8 of a synchrotron oscillation centered about the new synchronous phase. After the voltage is restored to V_0, during the time ($t_1 < t < t_2 = \frac{\tau_{s,h}}{4}$), the bunch executes oscillations about the original synchronous phase angle. If no other changes were made, then both the first and second moments (mean phase and bunch length) of the particle distribution would subsequently vary in time. Application of a second step change in voltage to 0.75 V_0 for a time $t_2 < t < t_3 = \frac{\tau_{s,l}}{8}$ shifts again the rf bucket and the bunch oscillates again around the new synchronous phase for 1/8 of a synchrotron period. With a perfectly linear rf system as assumed, the bunch centroid would return to $\delta = 0$ and $\phi = 0$ as initially, and would remain there indefinitely.

b) With a finite bunch length, the distribution of particles at t_3 is mismatched in the original phase space. The different particles have therefore different trajectories in longitudinal phase space. Since the synchrotron tune is approximately the same for all particles, by waiting an appropriate time, eventually (within a fraction of a synchrotron period) the particles will be aligned vertically in phase space with a significantly smaller bunch length, but with an increase in energy variation between particles. In this example with a two step changes in the applied voltage, the first moment is restored

while the second moment varies in time; the bunch rotates in phase space with the centroid position at $\delta = 0$ and $\phi = 0$.

Bunch precompression was used in the SLC damping rings to decrease the particle losses in the extraction line prior to injection into the main linac. By decreasing the bunch length at extraction, the energy variation along the bunch introduced by a downstream compressor was reduced. This in turn translated to a smaller dispersive beam size in the transport line which had a restricted horizontal aperture. A slightly different type of bunch precompression is also used at DESY in the PETRA accelerator, in order to reduce the bunch length at extraction for injection into the HERA accelerator for better capture efficiency. Here, two step changes are applied to the rf phase. The first shifts the rf phase by π, which places the beam distribution next to the unstable fixed point. The ensuing slow motion of particles along the separatrices translates into a mismatch, when the second step change moves the phase back to the original position.

8.3 Harmonic Cavities

a) From $eV(0) = U$, $\mathrm{d}V(t)/\mathrm{d}t|_{t=0} = 0$, and $\mathrm{d}^2V(t)/\mathrm{d}t^2|_{t=0} = 0$, we obtain

$$\sin\phi_1 + k\cos n\phi_n = \frac{U}{e\hat{V}} \tag{12.82}$$

$$\cos\phi_1 + kn\cos n\phi_n = 0 \tag{12.83}$$

$$\sin\phi_1 + kn^2\cos n\phi_n = 0\,. \tag{12.84}$$

Combining the last two equations yields

$$\tan n\phi_n = \frac{\tan\phi_1}{n}\,, \tag{12.85}$$

or

$$\sin n\phi_n = \frac{\tan\phi_1}{\sqrt{n^2 + \tan^2\phi_1}}\,, \tag{12.86}$$

and

$$k = -\frac{\cos\phi_1}{n\cos n\phi_n}\,. \tag{12.87}$$

Inserting these relations into (12.82), we get

$$\sin\phi_1 = \frac{n^2}{n^2-1}\frac{U}{e\hat{V}}\,, \tag{12.88}$$

so that (12.86) becomes

$$\tan n\phi_n = \frac{nU/(e\hat{V})}{\sqrt{(n^2-1)^2 - (n^2U/(e\hat{V}))^2}}\,. \tag{12.89}$$

Finally, using this result in (12.87) we obtain for the square of the relative voltage amplitude

$$k^2 = \frac{1}{n^2} - \frac{n^2}{(n^2-1)^2}\left(\frac{U}{e\hat{V}}\right)^2\,. \tag{12.90}$$

b) As the ratio of radiative losses to primary rf voltage varies from zero (proton beam limit) to slightly less than one, the phase ϕ_1 changes from 0 to almost $\pi/2$, whereas the optimum phase ϕ_n much more slowly increases from $-\pi$ towards $-\pi/2$.

8.4 Minimum Voltage Required for Beam Storage

a) The total radiated power for 10^{11} particles is 16.9 kW.

b) The energy lost per turn is 44.3 keV. Thus, at 44.3 kV voltage the beam could no longer be captured. The synchronous phase at this voltage is $\pi/2$ measured with respect to the zero crossing.

c) Lowering the cavity voltage limits the maximum beam energy and may also reduce the number of particles that can be captured. Note that a large change in voltage is required in order to significantly vary the bunch length. On the other hand, the use of harmonic cavities does not affect the available capture voltage.

8.5 Phase Shift along a Bunch Train

During the passage of the bunch train, the additional voltage $V_{\mathrm{beam}} = ZI_{\mathrm{b}}$ is applied to the cavity, where Z is the impedance, and $I_{\mathrm{b}} = 2I_{\mathrm{dc}}$ is the beam current at the rf frequency. The cavity response is

$$\Delta V = V_{\mathrm{beam}}\left(1 - e^{-\frac{t_{\mathrm{train}}}{\tau_f}}\right) \approx V_{\mathrm{beam}} t_{\mathrm{train}}/\tau_f\,, \tag{12.91}$$

where the cavity fill time is 2 μs. The beam induced voltage is $V_{\mathrm{beam}} = 5$ MV. The change in the cavity voltage along the bunch train amounts to $\Delta V = 775$ kV. The synchronous phase shift along the train can be estimated as

$$\Delta\phi \approx \frac{\Delta V}{V} \approx 0.0775 \text{ rad} = 4.4 \text{ deg}\,. \tag{12.92}$$

9.1 Septum Fields for Injection and Extraction

The beam separation at the septum can be written as

$$x_{\mathrm{sep}} = \sqrt{\beta_{\mathrm{kic}}\beta_{\mathrm{sep}}}\sin\mu\ \theta_{\mathrm{kic}}\,, \tag{12.93}$$

where the kick angle is

$$\theta_{\rm kic} = \frac{B_{\rm kic} L_{\rm kic}}{(B\rho)}\,, \tag{12.94}$$

with $(B\rho)$ the magnetic rigidity, $L_{\rm kic}$ the length of the kicker, and $B_{\rm kic}$ the kicker field. We should fulfill

$$x_{\rm sep} > n_s \sigma_x = n_{\rm sep} \sqrt{\beta_{\rm sep} \frac{\epsilon_{x,N}}{\gamma}} \tag{12.95}$$

Inserting (12.93) and solving for $B_{\rm kic}$ we find

$$B_{\rm kic} = \frac{n_s (B\rho) \sqrt{\epsilon_{x,N}/\gamma}}{\sqrt{\beta_{\rm kic}} L_{\rm kic} \sin\mu}\,. \tag{12.96}$$

Finally using $(B\rho) \approx 3.356{\rm Tm}\ E/{\rm GeV}$ and $\gamma \approx E/{\rm GeV}$ we estimate

$$B_{\rm kic} \approx 3.356{\rm Tm} \frac{n_s \sqrt{\epsilon_{x,N}}}{\sqrt{\beta_{\rm kic}} L_{\rm kic} \sin\mu} \sqrt{\frac{E}{\rm GeV}}\,. \tag{12.97}$$

Assuming $n_s = 10$, $\beta_{\rm kic} = 100$ m, $\mu = \pi/2$, $L_{\rm kic} = 5$ m, and $\epsilon_{x,N} = 4$ μm, the magnetic field $B_{\rm kic}$ required at a beam energy of 10 GeV and at 10 TeV is 4.3 mT and 0.134 T, respectively.

9.2 Emittance Dilutions due to Injection Errors

a) We estimate the emittance resulting from an injection error x_0 after filamentation as

$$\epsilon_x \approx \frac{x_0^2}{2\beta_x}\,. \tag{12.98}$$

For $x_0 = 1$ mm and $\beta_x = 100$ m, this gives $\epsilon_x \approx 5$ nm. The corresponding normalized emittances for various particles and energies are listed in the following table, along with the typical design emittances.

	10 GeV	1 TeV	Design norm. emittance
p	55 nm	5.5 μm	3.75 μm
μ	473 nm	47 μm	50 μm
e	98 μm	9.8 mm	3 nm

Obviously, the emittance dilution becomes more severe at higher energies.

b) The rms beam size at $\beta_x = 100$ m is 224 μm for a 7-TeV proton beam (LHC), 554 nm for a 500-GeV electron beam (NLC), and 514 μm for a 2-TeV muon beam (MC).

9.3 Filamentation

The filamented 'point bunch' occupies a circle in phase space. Using $x = r\cos\phi$ and $\phi = \arccos(x/r)$ the projected density is

$$\frac{{\rm d}N}{{\rm d}x} = \frac{{\rm d}N}{{\rm d}\phi} \frac{{\rm d}\phi}{{\rm d}x}\,. \tag{12.99}$$

Now $\mathrm{d}N/\mathrm{d}\phi = 2/(2\pi) = 1/\pi$, and $\mathrm{d}\phi/\mathrm{d}x = 1/\sqrt{r^2 - x^2}$, so that the projected density becomes

$$\frac{\mathrm{d}N}{\mathrm{d}x} = \frac{1}{\pi\sqrt{r^2 - x^2}}\,. \tag{12.100}$$

9.4 Particle Impact for Slow Extraction

The change in the action variable over three turns is

$$\Delta I = \frac{\partial H}{\partial \psi} 6\pi = \frac{3}{8}(2I)^{3/2}|\tilde{K}_s|\cos(3\psi + \theta_0)2\pi\,. \tag{12.101}$$

On the resonance near the unstable fixed point, but with an asymptotic angle for large amplitudes of $\psi \approx \pm\pi/6$ instead of 0, the cosine factor is approximately constant, equal to 1.

Considering only every 3rd turn, the amplitude at the septum is

$$x_{\mathrm{sep}} = \sqrt{2\beta_{\mathrm{sep}} I}\cos\psi \approx \sqrt{2\beta_{\mathrm{sep}} I}\,, \tag{12.102}$$

where we have roughly approximated $\cos\pi/6 \approx 1$. The change in amplitude at the septum over three turns becomes

$$\Delta x_{\mathrm{sep}} \approx \sqrt{\frac{\beta_{\mathrm{sep}}}{2I}}\Delta I_{\mathrm{sep}}\,, \tag{12.103}$$

which, after inserting (12.101) and (12.102), becomes

$$\Delta x_{\mathrm{sep}} = \frac{3\pi}{4}(2I)|\tilde{K}_s|\sqrt{\beta_{\mathrm{sep}}} = \frac{3\pi}{4}\frac{x_{\mathrm{sep}}^2}{\beta_{\mathrm{sep}}^{1/2}}|\tilde{K}_s|\,. \tag{12.104}$$

9.5 Crystal Channeling

From (9.23), the critical radius is

$$R_c \approx 0.4\mathrm{m}\; p[\mathrm{TeV}/c]\,. \tag{12.105}$$

This translates into a maximum bending angle over the length l of

$$\theta \leq \frac{l}{R_c}\,, \tag{12.106}$$

which for $l = 3$ cm at 7 TeV/c amounts to $\theta \leq 11$ mrad.

10.1 Electrostatic Lenses and Muon Storage Rings

If $\gamma = \sqrt{1 + \frac{1}{a_\mu}}$, we have $(\gamma^2 - 1) = 1/a_\mu$, and the coefficient multiplying the electric field in the equation for the spin precession is zero:

$$\left(a_\mu\gamma - \frac{\gamma}{\gamma^2 - 1}\right) = (a_\mu\gamma - a_\mu\gamma) = 0\,. \tag{12.107}$$

10.2 Spinors

a) Letting

$$\begin{aligned} \Psi &= \begin{pmatrix} a \\ b \end{pmatrix} \\ \Psi^\dagger &= (a^*,\ b^*)\,, \end{aligned} \tag{12.108}$$

where a and b are to be determined,

$$\begin{aligned} \Psi^\dagger \sigma_x \Psi &= a^* b + b^* a \\ \Psi^\dagger \sigma_s \Psi &= -\mathrm{i} a^* b + \mathrm{i} b^* a \\ \Psi^\dagger \sigma_y \Psi &= |a|^2 - |b|^2\,. \end{aligned} \tag{12.109}$$

Setting these equal to the spin basis vector of interest and using the normalization $|\Psi|^2 = 1$,

$$\begin{aligned} \Psi_x &= \frac{1}{\sqrt{2}} \begin{pmatrix} 1 \\ 1 \end{pmatrix} \\ \Psi_s &= \frac{1}{\sqrt{2}} \begin{pmatrix} 1 \\ i \end{pmatrix} \\ \Psi_y &= \begin{pmatrix} 1 \\ 0 \end{pmatrix}\ . \end{aligned} \tag{12.110}$$

b) For example,

$$\sigma_s {\sigma^\dagger}_s = \begin{pmatrix} 0 & -\mathrm{i} \\ \mathrm{i} & 0 \end{pmatrix} \begin{pmatrix} 0 & \mathrm{i} \\ -\mathrm{i} & 0 \end{pmatrix}^t = \begin{pmatrix} 1 & 0 \\ 0 & 1 \end{pmatrix} = I\,, \tag{12.111}$$

where ${\sigma^\dagger}_s = \sigma_s$ is obvious.

c) For example, with equal indices,

$$\sigma_s \sigma_s = \delta_{ss} I + \mathrm{i} \Sigma_m \epsilon_{ssm} \sigma_m = I\,, \tag{12.112}$$

since $\delta_{ss} = 1$ and $\epsilon_{ssm} = 0$ for all m. Squaring σ_s gives the same result.

With unequal indices, for example,

$$\begin{aligned} \sigma_y \sigma_s &= \delta_{ys} I + \mathrm{i} \Sigma_m \epsilon_{ysm} \sigma_m \\ &= \mathrm{i}(\epsilon_{ysx} \sigma_x + \epsilon_{yss} \sigma_s + \epsilon_{ysy} \sigma_y) \\ &= \mathrm{i} \epsilon_{ysx} \sigma_x = -\mathrm{i} \sigma_x\,, \end{aligned} \tag{12.113}$$

and $\epsilon_{ysx} = -1$. Direct multiplication of $\sigma_y \sigma_s$ gives the same result.

10.3 Spin Precession in Solenoidal Fields

a) From (10.2) and (10.7),

$$\Omega = -\frac{e}{\gamma m}(1 + G) B_z\,, \tag{12.114}$$

With $\boldsymbol{B} = B_z\hat{s}$, $\boldsymbol{\beta} = \beta\hat{s}$, and $\boldsymbol{E} = 0$, and a solenoidal field of length l,

$$\phi = \Omega t = -\frac{e}{\gamma mc}\frac{l}{\beta}(1+G)B_z\,. \tag{12.115}$$

b) The Lorentz force acting on the particle is $F_L = e\beta cB$ and the centrifugal force $F_c = m\gamma c^2\beta^2/\rho$. The combination gives

$$B\rho = \frac{\beta E}{ec} = \frac{\beta\gamma mc}{e}\,. \tag{12.116}$$

Direct substitution in (12.115) yields

$$\phi = -\frac{B_z l}{B\rho}(1+G)\,. \tag{12.117}$$

c) With $T = 100$ MeV, we obtain $p = 444$ MeV/c and $B\rho = 444/299.8 = 1.48$ T-m. So the required integrated field strength is $B_z l = 1.66$ T-m.

10.4 Periodic Spin Motion

From (10.24) and the definition of the directional cosines,

$$\begin{aligned} M &= e^{-\mathrm{i}\pi\nu_s(\sigma\cdot\hat{n}_0)} = I_2\cos\pi\nu_s - \mathrm{i}(\sigma\cdot\hat{n}_0)\sin\pi\nu_s \\ &= I_2\cos\pi\nu_s - \mathrm{i}(\sigma_x\cos\alpha_x + \sigma_s\cos\alpha_s + \sigma_y\cos\alpha_y)\sin\pi\nu_s. \end{aligned} \tag{12.118}$$

Substituting the Pauli matrices gives the result directly.

10.5 SLC '3-state experiment'

Since the spin transport through the arcs is a pure precession, the polarization vector is simply rotated. In particular, using the inverse transformation we can back-propagate the direction of longitudinal polarization at the collision point to the coordinate system of the incoming beam. Using spherical coordinates, we may express the orientation of the back-propagated polarization vector at the injection point as

$$\boldsymbol{P} = P_{\mathrm{IP}}(\sin\phi\sin\theta, \cos\phi\sin\theta, \cos\theta)\,. \tag{12.119}$$

Now, measuring the longitudinal polarization at the IP for the three initial states

$$\begin{aligned} \boldsymbol{P}_1 &= (1,0,0) \\ \boldsymbol{P}_2 &= (0,1,0) \\ \boldsymbol{P}_3 &= (0,0,1) \end{aligned} \tag{12.120}$$

determines the three components of $\boldsymbol{S}$ in (12.119). Now the magnitude of the polarization vector at the IP is simply the sum in quadrature of the three values measured:

$$||P_{\mathrm{IP}}|| = \sqrt{(\boldsymbol{P}_1\cdot\boldsymbol{P}_{\mathrm{IP}})^2 + (\boldsymbol{P}_2\cdot\boldsymbol{P}_{\mathrm{IP}})^2 + (\boldsymbol{P}_3\cdot\boldsymbol{P}_{\mathrm{IP}})^2}\,. \tag{12.121}$$

At the SLC, this 3-state experiment was applied regularly, e.g., every few months, in order to monitor the IP polarization and to optimize the orientation of the spin vector at the collision point. The initial direction of the polarization was varied by means of solenoidal spin rotators located in the transfer line between the electron damping ring and the SLC linac.

10.6 Type-3 Snakes

a) With regard to the orbit, the sum of the horizontal and vertical deflections is zero. With the beam momentum purely longitudinal, there is no deflection due to the longitudinal fields. The type-3 snake is therefore optically transparent with respect to the angle (though in this example, a net offset is introduced). The spin matrices, however, do not commute. The matrix product is

$$\left(e^{\mathrm{i}\frac{\phi}{4}\sigma_x}e^{-\mathrm{i}\frac{\chi}{4}\sigma_s}e^{-\mathrm{i}\frac{\phi}{4}\sigma_x}\right)e^{\mathrm{i}\frac{\chi}{4}\sigma_s}\left(e^{\mathrm{i}\frac{\phi}{4}\sigma_x}e^{-\mathrm{i}\frac{\chi}{4}\sigma_s}e^{-\mathrm{i}\frac{\phi}{4}\sigma_x}\right), \qquad (12.122)$$

where σ_x and σ_y are the Pauli matrices. This product can be evaluated using the expansion (12.118) and matrix multiplication. For the given case, the product of the spin matrices is different from unity, if neither χ nor ϕ equal 0 or 2π.

b) The horizontal orbit and the spin orientations for the case $\phi = \chi = \pi$ are shown in Fig. 12.3.

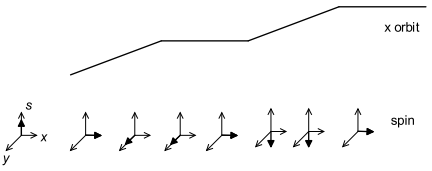

Fig. 12.3. Horizontal orbit and spin orientation along the beam line of Ex. 10.6 with $\phi = \chi = \pi$

This example is derived from experience at the IUCF cooler ring. There, the longitudinal fields were provided by the main cooling solenoid together with the compensating solenoids (1 on each side of the cooling region). The orbital displacements and dipolar deflections arose from the bending fields used to align the proton beam with the cooling electrons.

11.1 Longitudinal Damping Rate with Beam Cooling

The centroid motion is characterized by the centroid momentum $P = (p_1 + p_2)/2$, which fulfills the equation

$$\frac{\mathrm{d}P}{\mathrm{d}t} = \frac{1}{2}\frac{\mathrm{d}(p_1 + p_2)}{\mathrm{d}t} = -\lambda(p_1 + p_2) = -2\lambda P\,. \qquad (12.123)$$

From this we obtain the damping rate

$$\frac{1}{\tau_P} = \frac{1}{P}\frac{\mathrm{d}P}{\mathrm{d}t} = -2\lambda\,. \qquad (12.124)$$

Since there are only two particles, we can define the momentum spread as the difference between the two particle momenta: $p_{\rm spr} = p_1 - p_2$. The time derivative of $p_{\rm spr}$ is

$$\frac{\mathrm{d}p_{\rm spr}}{\mathrm{d}t} = \frac{\mathrm{d}(p_1 - p_2)}{\mathrm{d}t} = -\lambda(p_1 - p_2) = 0\,. \tag{12.125}$$

Hence, the momentum spread is unchanged by the cooling.

11.2 Temperature of a Cooled Beam

a) We have

$$\begin{aligned} T_x &= \frac{\langle p_x^2\rangle}{k_B m} = \frac{(mc\beta\gamma x')^2}{k_B m} \\ &= \frac{c^2 m \epsilon_{x,N}\beta\gamma}{k_B \beta_x} \end{aligned} \tag{12.126}$$

$$\begin{aligned} T_{||} &= \frac{\langle \Delta p_{||}^2\rangle}{k_B m} = \frac{mc^2\left\langle \frac{\Delta p_{||}^2}{(mc)^2}\right\rangle}{k_B} \\ &= \frac{mc^2\beta^2\left\langle \frac{\Delta p_{\rm lab}^2}{(\gamma\beta mc)^2}\right\rangle}{k_B} = \frac{mc^2\beta^2\left\langle \frac{\Delta p_{\rm lab}^2}{p_{\rm lab}^2}\right\rangle}{k_B} \\ &= \frac{mc^2\beta^2\sigma_p^2}{k_B}\,, \end{aligned} \tag{12.127}$$

where we have related the momentum deviation in the beam frame and in the laboratory frame via $\Delta p_{\rm lab} = \gamma\Delta p_{||}$.

b) The velocity and energy of the proton beam follow from $\beta\gamma = 0.7$ or $\beta = 0.57$. The horizontal temperature is $k_B T_x = 32.8$ eV ($T_x = 404$ kK); the longitudinal temperature $k_B T_{||} = 309$ eV ($T_{||} = 3.8$ MK).

The transverse temperature of the electron beam is $T_x = 1230$ K ($k_B T_x = 0.1$ eV). For the longitudinal plane, we use the relation $\Delta p/p = (1/\beta^2)\Delta E/E$; The energy difference ΔE between particles is unchanged by the acceleration, so that $\langle \Delta E\rangle = k_B T^c/2$. Further assuming a Gaussian distributions for the momenta, one can show that $\langle (\Delta E)^2\rangle = 4\langle \Delta E\rangle^2 = (k_B T^c)^2$. Combining these relations and the definition of $T_{||}$, we find

$$T_{\parallel} = \frac{(k_B T^c)^2}{\beta^2\gamma^2 mc^2}\,. \tag{12.128}$$

For 100 kV accelerating voltage, we have $\gamma \approx 1.2$, $\beta \approx 0.55$, and $T_{\parallel} \approx 4 \times 10^{-8}$ eV. Thus, after acceleration the longitudinal temperature of the electron beam is much smaller than its transverse temperature.

c) For $T_x = 1230$ K, the transverse Debye shielding length (11.22) is $r_D \approx 136$ μm.

d) For a field B of 500 Gauss the electron cyclotron period is $T_{\rm cycl} = 2\pi m_e/(eB) \approx 0.7$ ns. The transverse velocity of the proton beam is

$$v_x^2 \approx \frac{k_B T_x}{m}\,, \tag{12.129}$$

which yields $v_x \approx 2.4 \times 10^6$ m/s. Then the typical impact time is $t_{\rm impact} \sim r_D/u_\perp \sim r_D/v_x \approx 6 \times 10^{-11}$ s. For these parameters, the impact time is about 10 shorter than the cyclotron period. For a field of 5 kG the two times would be equal.

11.3 Recombination of Ion Beams during Electron Cooling

According to (11.27)

$$\frac{1}{\tau} \propto \frac{Z^2}{A}\,. \tag{12.130}$$

Thus the cooling time for fully stripped lead ions is $82^2/207$ times that for protons, or $\tau_{Pb} \approx 308$ μm. The electron capture rate scales as (11.28)

$$\frac{1}{\tau_r} \propto Z^2\,. \tag{12.131}$$

Hence, for the Pb ions it is 15 s.

The fraction of lead ions that would be lost by recombination during one cooling time is

$$\frac{\Delta N}{N} \approx \frac{308\ \mu\text{s}}{15\ \text{s}} \approx 2 \times 10^{-5}\,. \tag{12.132}$$

11.4 Electron-Beam Energy for Electron Cooling

The relativistic Lorentz factor γ should be the same for both beams. Hence, the electron-beam energy required to cool the 7-TeV LHC proton beam is about 3.8 GeV.

11.5 Derivation of the Debye Length

We denote the change in potential experienced by electrons near a single ion charge by $\phi(r)$, where r is the distance from the ion. In thermal equilibrium the electron density is described by

$$n(r) = n_0 e^{-\frac{e\phi(r)}{k_B T}} \approx n_0 \left(1 - \frac{e\phi(r)}{k_B T}\right)\,, \tag{12.133}$$

so that the deviation from the unperturbed density n_0 is

$$\Delta n(r) \approx -n_0 \frac{e\phi(r)}{k_B T}\,. \tag{12.134}$$

Noting that the electron charge is $-e$, the Laplace equation for the perturbed potential, ϕ, in the vicinity of the ion is

$$\frac{\partial^2 \phi(r)}{\partial r^2} = \frac{\Delta n e}{\epsilon_0} = -\left(n_0 \frac{e^2}{k_B T \epsilon_0}\right)\phi\,, \tag{12.135}$$

with the solution

$$\phi = \phi_0 e^{-\sqrt{\frac{n_0 e^2}{k_B T \epsilon_0}} r} = \phi_0 e^{-\frac{r}{r_D}} , \tag{12.136}$$

where the Debye shielding length r_D equals

$$r_D = \left(\frac{k_B T}{4\pi n_0 m c^2 r_e} \right)^{1/2} . \tag{12.137}$$

11.6 Interaction Probability with Electron Cooling

The ion velocity u follows from

$$u^2 = \frac{k_B T}{m} = c^2 \beta\gamma \frac{\epsilon_N}{\beta_x} \approx \left(4 \times 10^5 \text{ m/s} \sqrt{\beta\gamma} \right)^2 , \tag{12.138}$$

where β and $\gamma = 1/(1-\beta^2)$ are the relativistic factors. Using the minimum impact parameter $\rho_{\min}$ from (11.23), we obtain an interaction time of

$$t_{\text{int}} \approx \frac{\rho_{\min}}{u} = \frac{r_e c^2}{u^3} = (\beta\gamma)^{-3/2} \times 4 \times 10^{-15} \text{ s} . \tag{12.139}$$

Denoting the length of the cooling section by l, the travel time is

$$t_{\text{trav}} \approx \frac{l}{\beta c} = 3 \times 10^{-8}/\beta \text{ s} . \tag{12.140}$$

For the parameters chosen, the two times will only be equal for an extremely small value of β (about 2×10^{-14}), which will not occur in practice. However, the interaction time increases with decreasing ion-beam emittance.

11.7 Beam Temperature with Ion-Beam Laser Cooling

(a) From (11.47) we have

$$\Delta\beta \approx \frac{\Delta\omega'}{\omega'} , \tag{12.141}$$

which, for a laser tuning range of $\Delta f = 20$ GHz and a laser wavelength of $\lambda = 280$ nm, gives $\Delta\beta \approx 1.9 \times 10^{-5}$. The velocity of the ion beam is $\beta \approx (100 \text{ kV}/(\frac{1}{2} m_p A c^2))^{1/2} \approx 3 \times 10^{-3}$, so that $\Delta\beta/\beta \approx 6 \times 10^{-3}$.

(b) The minimum temperature according to (11.49) is 120 μK which corresponds to 10^{-8} eV. The temperature is also limited by the recoil energy acquired in the beam frame when absorbing a single photon, which is $(1/2) m_{\text{ion}} v_r^2$. Inserting v_r from (11.48), this amounts to only 5 μK or 4^{10} eV. The larger of these two limits applies, namely 120 μK.

11.8 Damping Times with Electron-Beam Laser Cooling

From (11.55) we get $n_d \approx 1600$ turns. The equivalent damping time for an average ring radius ρ of 1 m is

$$\tau_d = n_d \left(\frac{c}{2\pi\rho} \right) \approx 34 \text{ μs} . \tag{12.142}$$

This is two orders of magnitude smaller than in conventional storage rings.

11.9 Equilibrium Emittances with Electron-Beam Laser Cooling

The equilibrium emittance is given by (11.61)

$$\epsilon_{x,y,N} = \frac{3}{10}\frac{\lambda_c}{\lambda_L}\beta^*_{x,y} \approx 7 \times 10^{-9}\ \mathrm{m}\,, \tag{12.143}$$

and the relative energy spread by

$$\sigma_\delta = \sqrt{\frac{7}{5}\frac{\lambda_c}{\lambda_L}\gamma} \approx 2.6\%\,. \tag{12.144}$$

11.10 Damping Rates and Equilibrium Emittances with Ionization Cooling

(a) From $(\gamma - 1)m_\mu c^2 = 150$ MeV we deduce $\gamma \approx 2.42$. The first term on the right hand side of (11.113) describes the damping. Its average rate is

$$\lambda = \frac{1}{\epsilon_N}\frac{\mathrm{d}\epsilon_N}{\mathrm{d}s} = -\frac{l_{H_2}}{l_{\mathrm{cool}}}\frac{1}{\beta^2}\frac{\mathrm{d}E_\mu}{\mathrm{d}s}\frac{1}{E_\mu} \approx -0.074\ \mathrm{m}^{-1}\,, \tag{12.145}$$

where l_{H_2} and l_{cool} denote the length of the hydrogen cell and the length of the entire cooling stage, respectively. The emittance reduction in a section of length $l_{\mathrm{cool}} = 10$ m is a factor $\exp(\lambda l_{\mathrm{cool}}) \approx 0.48$.

(b) The total length required for a factor 10 emittance reduction is

$$l_{\mathrm{tot}} = -\frac{1}{\lambda}\ln(10) \approx 31\ \mathrm{m}\,, \tag{12.146}$$

or about three 10-m long stages. The muon lifetime in the laboratory system is $\tau_{\mathrm{lab}} = \gamma\tau_{\mu,0} \approx 5.2$ μs, where $\tau_{\mu,0}$ denotes the muon lifetime at rest. The fraction of muons left after traversing $l = 500$ m at 150 MeV is $\exp(-l/(\beta c\tau_{\mathrm{lab}})) \approx 0.7$, or 70%.

(c) The minimum normalized emittance is reached when the time derivative on the left-hand side of (11.113) approaches zero. We can solve the right-hand side for the final emittance and obtain

$$\epsilon_N = \frac{1}{\beta}\frac{\beta_\perp}{2}\frac{(14\ \mathrm{MeV})^2}{(\mathrm{d}E_\mu/\mathrm{d}s)m_\mu c^2 L_R} \approx 4 \times 10^{-4}\ \mathrm{m}\,. \tag{12.147}$$

(d) We first discuss the damping term. The trajectory slope x' is related to the horizontal and longitudinal momenta p_x and p_0 via

$$x' = \frac{p_x}{p_0}\,, \tag{12.148}$$

and due to the ionization energy loss in the direction of the trajectory and re-acceleration in the longitudinal direction over a distance Δs it changes as

$$\Delta x' = -\frac{p_x}{p_0^2}\frac{\Delta p_0}{\Delta s}\Delta s\,. \tag{12.149}$$

Now, $\Delta p_0/\Delta s = (\mathrm{d}E_\mu/\mathrm{d}s)/(\beta c)$, so that

$$\frac{\Delta x'}{\Delta s} = -x' \frac{1}{\beta^2 \gamma m_\mu c^2} \frac{\mathrm{d}E_\mu}{\mathrm{d}s} \,. \tag{12.150}$$

The analogous equation applies in the vertical plane. From (1.15), the change in transverse (horizontal or vertical) action is

$$\frac{\Delta I_\perp}{\Delta s} = -\beta_\perp x'^2 \frac{1}{\beta^2 \gamma m_\mu c^2} \frac{\mathrm{d}E_\mu}{\mathrm{d}s} \,. \tag{12.151}$$

Since $\Delta \epsilon_N = \beta\gamma \langle \Delta I_\perp \rangle$, and $\epsilon_N = \beta\gamma \langle \beta_\perp x'^2 \rangle$ the damping term in (11.113) follows.

To derive the heating term we start from (1.15) and compute the change in action due to multiple scattering at an angle θ:

$$\Delta I_\perp = \frac{2\beta_\perp \theta(\alpha_\perp x + \beta_\perp x') + \beta_\perp^2 \theta^2}{2\beta_\perp} \,. \tag{12.152}$$

After averaging over the distribution (assuming random betatron phases) only the term quadratic in θ remains, or

$$\langle \Delta I_\perp \rangle = \frac{\beta_\perp \langle \theta^2 \rangle}{2} \,, \tag{12.153}$$

where $\langle \theta^2 \rangle$ is the squared rms scattering angle after a distance s. Inserting (11.114) for this angle, differentiating with respect to s, and noticing again that $\epsilon_N = \beta\gamma \langle \Delta I_\perp \rangle$, the previous equation is rewritten as

$$\begin{aligned} \frac{d\epsilon_N}{ds} &= \frac{\beta_\perp}{2} \frac{\beta\gamma \,(14 \text{ MeV})^2}{(\beta c p)^2} \frac{1}{L_R} \\ &= \frac{\beta_\perp}{2\beta^3} \frac{(14 \text{ MeV})^2}{E_\mu m_\mu c^2 L_R} \,, \end{aligned} \tag{12.154}$$

which equals the expression for the heating in (11.113).